Chemical Science

ROYAL SOCIETY OF CHEMISTRY

EDGE ARTICLE

View Article Online
View Journal | View Issue



Cite this: *Chem. Sci.*, 2022, **13**, 7014

All publication charges for this article have been paid for by the Royal Society of Chemistry

Received 1st April 2022
Accepted 20th May 2022

DOI: 10.1039/d2sc01876d

rsc.li/chemical-science

# Enantioselective assembly and recognition of heterochiral porous organic cages deduced from binary chiral components†

Chao Liu, Yucheng Jin, Dongdong Qi, Xu Ding, Huimin Ren, Hailong Wang * and Jianzhuang Jiang *

Chiral recognition and discrimination is not only of significance in biological processes but also a powerful method to fabricate functional supramolecular materials. Herein, a pair of heterochiral porous organic cages (HPOC-1), out of four possible enantiomeric products, with mirror stereoisomeric crystal structures were cleanly prepared by condensation occurring in the exclusive combination of cyclohexanediamine and binaphthol-based tetraaldehyde enantiomers. Nuclear magnetic resonance and luminescence spectroscopy have been employed to monitor the assembly process of HPOC-1, revealing the clean formation of heterochiral organic cages due to the enantioselective recognition of (*S*,*S*)-binaphthol towards (*R*,*R*)-cyclohexanediamine derivatives and *vice versa*. Interestingly, HPOC-1 exhibits circularly polarized luminescence and enantioselective recognition of chiral substrates according to the circular dichroism spectral change. Theoretical simulations have been carried out, rationalizing both the enantioselective assembly and recognition of HPOC-1.

## Introduction

Porous organic cages (POCs) are newly emerging attractive crystalline molecular materials with great application potential in the fields of storage and separation,[1] sensing,[2] and catalysis.[3] Their advantages originate from the intrinsic and extrinsic voids together with the functional groups attached on POCs. Thus far, molecular POCs are mainly formed from the self-assembly of discrete reactive building blocks driven by dynamic covalent chemistry (DCC) including the reactions of boronic acid condensation,[4] imine condensation,[5] and alkyne/alkene metathesis.[6] In particular, various amine- and aldehyde-decorated building blocks are available to assemble POC molecules with different cavities, dimensions, and topologies.[7] These discrete cage-like molecules obtained are engineered crystallographically to form porous assemblies (called POCs) through efficient supramolecular interactions, exhibiting huge adsorption capacity. In addition, the new application of POCs as a kind of unique synthon has been initiated by accommodating fine nanoparticles[8] and being fabricated into reticular frameworks[9] with the help of metal-coordination, covalent and hydrogen-bonding interactions.

Chirality is vital to biological processes and widely exists in various biological structures at the molecular level, including polysaccharides, proteins and DNA.[10] Incorporation of chirality into artificial functional materials provides new objectives towards chiral separation,[11] stereospecific catalysis,[12] chiral recognition,[13] and unique chiroptical properties.[14] Self-assembly depending on chiral recognition and discrimination has been used to prepare chiral functional supramolecular materials through noncovalent interactions such as electrostatic interactions,[15] π–π interactions,[16] hydrogen bonding,[17] and metal-coordination bonds.[18] In quite recent years, DCC-based self-sorting of POCs has been achieved using the racemic mixtures of enantiomers as building blocks, generating a few homochiral and heterochiral cages.[19] It is worth noting that all the thus far obtained heterochiral POCs are made up of enantiomers from only one component. More complicated heterochiral systems derived from the enantiomers of two or more components still remain unreported, to the best of our knowledge. As a consequence, investigation of complicated heterochiral cages and the corresponding applications is surely of significance for developing POCs and chirality chemistry.

Herein, we present the clean synthesis of heterochiral porous organic cages (HPOC-1) by enantioselective assembly of the enantiomer of a binaphthol-based tetraaldehyde with specific enantiopure cyclohexanediamine (CA). The corresponding self-assembly reaction kinetics has been tracked using luminescence and nuclear magnetic resonance (NMR)

*Beijing Advanced Innovation Center for Materials Genome Engineering, Beijing Key Laboratory for Science and Application of Functional Molecular and Crystalline Materials, Department of Chemistry and Chemical Engineering, School of Chemistry and Biological Engineering, University of Science and Technology Beijing, Beijing 100083, China. E-mail: hlwang@ustb.edu.cn; jianzhuang@ustb.edu.cn*

† Electronic supplementary information (ESI) available. CCDC 2114815 and 2114817. For ESI and crystallographic data in CIF or other electronic format see https://doi.org/10.1039/d2sc01876d

spectroscopy, revealing the clean formation of heterochiral porous organic cages due to the enantioselective recognition of the CA enantiomer towards the enantiomeric binaphthol-derived building block 5,5′-(6,6′-dichloro-2,2′-diethoxy-[1,1′-binaphthalene]-4,4′-diyl)diisophthalaldehyde (DBD). The crystal structures of the pair of heterochiral HPOC-1 enantiomers show precise sorting of two kinds of chiral building blocks. Interestingly, HPOC-1 displays circularly polarized luminescence (CPL). Furthermore, heterochiral HPOC-1 is able to enantioselectively recognize chiral substrates through circular dichroism (CD) spectral change due to the host–guest supramolecular interactions.

## Results and discussion

The synthetic route to POCs from tetraaldehydes and CA created by Cooper's group has provided diverse [3 + 6] tubular organic cages.[20] Towards synthesizing more complex heterochiral POCs with two different kinds of enantiomers from more than one component, pure chiral binaphthol-bearing building blocks (DBD) shown in Scheme 1 were prepared to react with cyclohexanediamine (CA). Four sets of combination for these enantiomeric building blocks of two compounds, namely [(*S*,*S*)-DBD + (*S*,*S*)-CA], [(*S*,*S*)-DBD + (*R*,*R*)-CA], [(*R*,*R*)-DBD + (*R*,*R*)-CA] and [(*R*,*R*)-DBD + (*S*,*S*)-CA], are expected to generate four heterochiral organic cages. Unfortunately, only the reaction between (*S*,*S*)-DBD and (*R*,*R*)-CA or (*R*,*R*)-DBD and (*S*,*S*)-CA was able to deliver clean (*S*,*R*)- and (*R*,*S*)-HPOC-1, respectively, on the basis of MS and NMR spectroscopic data, Table S1 and Fig. S1–S11.†

In order to understand the assembly process, time-dependent NMR spectra were collected for the system of (*S*,*S*)-DBD in 2.0 mL $CDCl_3$ containing 1.0 μL TFA with the addition of 2.0 equiv. of (*R*,*R*)-CA and (*S*,*S*)-CA, respectively, Fig. S12.† (*S*,*S*)-DBD showed one typical singlet peak at $\delta$ 10.26 ppm due to the aldehyde protons. In addition, methyl and methylene protons displayed peaks at $\delta$ 1.16 and 4.15 ppm, respectively. Following the addition of (*R*,*R*)-CA for 1.0 min, the proton signal of the aldehyde quickly disappeared. Instead, a doublet peak started to appear at $\delta$ 8.38 ppm due to the formation of imine bonds. After 20.0 min, the methyl proton signals moved towards high field of $\delta$ 0.27 ppm and methylene proton signals migrated to $\delta$ 3.00 and 3.28 ppm. The larger high-field movement indicates an increase in the density of the electron cloud around the methyl group, which further illustrates the location of ethoxy groups inside the cage molecule rather than outside the cage. After the proceeding of the reaction for 24.0 h, the $^1$H NMR spectrum of the reaction mixture is overall consistent with that of the as-synthesized (*S*,*R*)-HPOC-1, implying the clean generation of the heterochiral POC. This is verified by MALDI-TOF MS data with the observation of only one cage molecular ion peak at $m/z = 2495.6$, Fig. S13.† In contrast, introduction of (*S*,*S*)-CA led to complicated $^1$H NMR signals under the same reaction conditions, which are seriously different from those of (*S*,*R*)-HPOC, Fig. S14.† The assemblies in the reaction solution of (*S*,*S*)-DBD and (*S*,*S*)-CA have been analyzed using the MS result. Four molecular ion peaks at 2495.6, 3327.1, 4159.8 and 4992.2 are consistent with the molecular weight of [3 + 6], [4 + 8], [5 + 10] and [6 + 12] POCs, respectively, Fig. S13.† In addition, a complicated $^1$H NMR spectrum was obtained for the solid yielded from the reaction of four kinds of starting materials including (*S*,*S*)-DBD, (*R*,*R*)-DBD, (*S*,*S*)-CA, and (*R*,*R*)-CA (Fig. S15†), precluding the presence of pure self-sorting POCs. It is worth noting that the synthetic dynamics for the present POCs with both chiral aldehyde and chiral amine as the building blocks should be due to the enantioselective assembly mechanism, namely an enantiomer to enantioselectively recognize different kinds of chiral modules. This is different from that of self-sorting POCs with solely one kind of racemic molecule involving the chiral self-discrimination or self-recognition mechanism.[5b,19a–d,f]

In addition, fluorescence spectroscopy was used to trace the reaction dynamics of (*S*,*S*)-DBD with (*R*,*R*)-CA and (*S*,*S*)-CA, respectively, with a molar ratio of 1 : 2 in $CH_2Cl_2$, Fig. 1a–c. There is a slight emission band of DBD at *ca*. 502 nm. After the introduction of (*R*,*R*)-CA for 5.0 min, an obvious emission band was observed at *ca.* 418 nm. As time went on, the maximum

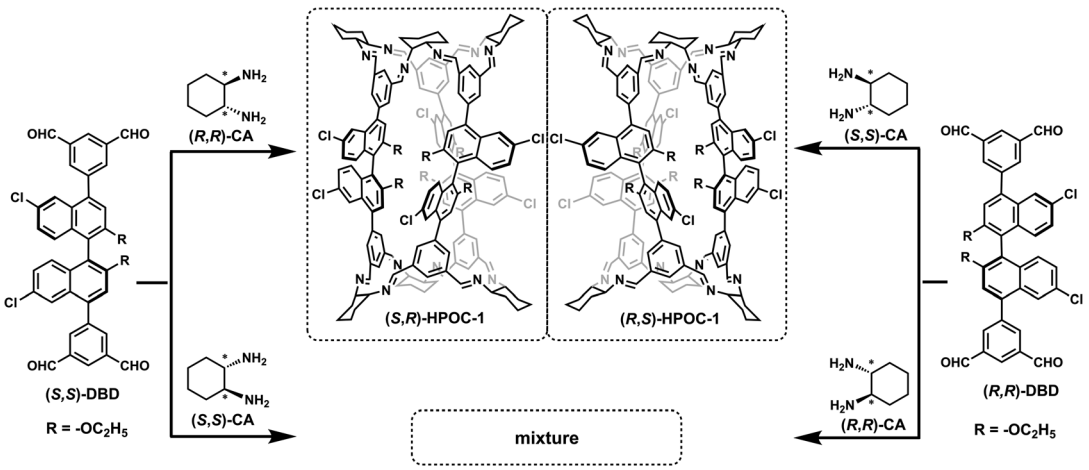


Scheme 1 Synthesis of heterochiral porous organic cage HPOC-1.

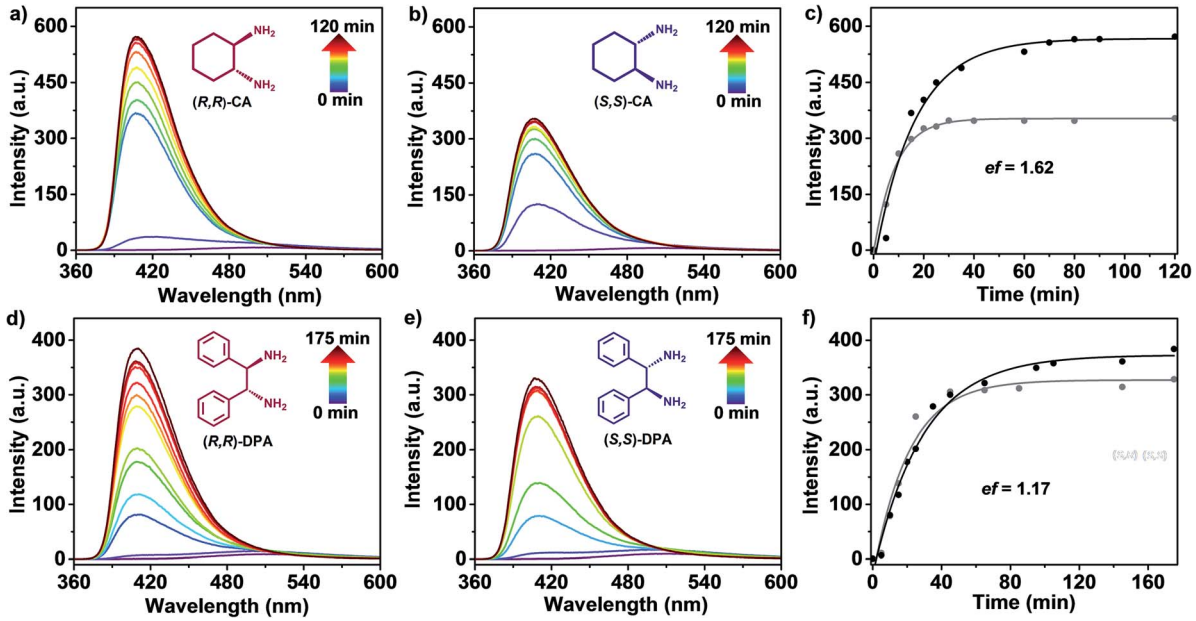


Fig. 1 (a and b) Fluorescence spectral changes of (*S*,*S*)-DBD (0.7 mM) in $CH_2Cl_2$ upon introduction of 2.0 equiv. of (*R*,*R*)-CA or (*S*,*S*)-CA. (c) Fluorescence intensity at 406 nm *vs.* reaction time of (*S*,*S*)-DBD with (*R*,*R*)-CA (black line) and (*S*,*S*)-CA (gray line). (d and e) Fluorescence spectral changes of (*S*,*S*)-DBD (0.7 mM) in $CH_2Cl_2$ upon introduction of 2.0 equiv. of (*R*,*R*)-DPA or (*S*,*S*)-DPA. (f) Fluorescence intensity at 406 nm *vs.* reaction time of (*S*,*S*)-DBD with (*R*,*R*)-DPA (black line) and (*S*,*S*)-DPA (gray line).

position of the emission band with gradually increased intensity slightly moved to 406 nm. After 60.0 min, the intensity remained constant. Such a phenomenon is also observed in the reaction system of (*S*,*S*)-DBD and (*S*,*S*)-CA, Fig. 1d–f. Differently, a shorter time of 30.0 min enabled a constant emission intensity at 406 nm maximum for the latter system. It is worth noting that the emission intensity at maximum for the former system was almost twice as big as that of the latter one. An enantiomeric fluorescence ratio (ef) value of 1.62 was therefore determined based on the division of maximum intensity of the former system by that of the latter one, confirming the higher enantioselectivity of (*S*,*S*)-DBD towards (*R*,*R*)-CA, rather than (*S*,*S*)-CA, to form pure [3 + 6] POC. When (*R*,*R*)-DBD was used, a similar phenomenon was found upon the addition of (*S*,*S*)-CA and (*R*,*R*)-CA, respectively, and the ef is calculated as 1.82, Fig. S16.† This value is similar to the ef of (*S*,*S*)-DBD. These results demonstrate the moderate enantioselectivity between these two chiral building blocks during the reaction.[13c,h]

Density functional theory (DFT) calculations were performed on (*S*,*R*)-HPOC-1 and (*S*,*S*)-HPOC-1 (assembled from (*S*,*S*)-DBD + (*S*,*S*)-CA) towards understanding the clean generation of the former heterochiral POC associated with enantioselective recognition between two kinds of enantiomeric building blocks. The simulated formation energy for (*S*,*R*)-HPOC-1 is $-132.4$ kcal mol$^{-1}$, much smaller than that for the latter species ($-71.5$ kcal mol$^{-1}$), hinting at the more favorable formation of the former cage from a thermodynamics perspective. In the present case, the optimized structure of (*S*,*R*)-HPOC-1 exhibits less variation in bond length for the cyclohexanediimine moiety than that of (*S*,*S*)-HPOC-1 (Fig. S17 and Table S2†), indicating the more stable structure of the former POC. To further confirm this point, theoretical simulation was also carried out on another heterochiral POC, HPOC-2 derived from the reaction between DBD and 1,2-diphenylethylamine (DPA) enantiomers. The formation energy of (*S*,*R*)-HPOC-2 ($-137.3$ kcal mol$^{-1}$), derived from (*S*,*S*)-DBD and (*R*,*R*)-DPA, was revealed to be smaller than that of (*S*,*S*)-HPOC-2 ($-131.7$ kcal mol$^{-1}$), assembled from (*S*,*S*)-DBD and (*S*,*S*)-DPA, further supporting the present clean generation of heterochiral POCs due to the enantioselective assembly mechanism. These results agree well with the experimental findings that [3 + 6] topological (*S*,*R*)-HPOC-2 has been cleanly generated according to NMR and MS data, Fig. S18 and S19.† However, the small enantiomeric fluorescence ratio of 1.17 for (*S*,*S*)-DBD toward (*R*,*R*)-DPA and (*S*,*S*)-DPA, Fig. 1f, indicates the weak selectivity of the enantioselective recognition process occurring in the generation of the latter heterochiral POCs in comparison with HPOC-1.

To detect the structural information of the heterochiral cages, colourless single crystal enantiomers of HPOC-1 were surveyed using a single crystal X-ray diffraction instrument, Fig. 2a and Table S3.† Both enantiomers crystallize in the monoclinic system with a chiral $P2_1$ space group, and each unit cell is made up of two cage molecules. The detailed structures of these two compounds were described with (*S*,*R*)-HPOC-1 assembled from (*S*,*S*)-DBD and (*R*,*R*)-CA as a typical representative. As expected, it inherits the [3 + 6] cage structural characteristics, possessing three binaphthol segments and six chiral diamines *via* imine connection. The length of this cage is about 24.4 Å, Fig. 2a. Although the cage cavity is crowded due to the ethoxy side chains, the solvent-accessible surface is computed to be 32.4% using Platon software.[21] The Flack parameters for the resolved single crystal structures of (*S*,*R*)-HPOC-1 and (*R*,*S*)-

HPOC-1 are 0.049(13) and 0.035(7), respectively, illustrating the enantiopurity of these two newly obtained POCs. As a result, the CD spectra were comparatively studied with reference to those of DBD, Fig. 2b and S20.† (*S*,*S*)-DBD shows a positive CD band from 240 to 260 nm and a negative band from 260 to 360 nm. The enantiomer exhibits mirror CD bands due to the completely inverse Cotton effect. After the formation of (*S*,*R*)-HPOC-1, three CD bands, namely a positive band in the range of 240–260 nm and two negative bands at 260–280 nm and 280–360 nm, respectively, were observed. The newly observed negative band at 260–280 nm might be the consequence of imine band formation from (*R*,*R*)-CA reacting with the (*S*,*S*)-DBD moiety. This is consistent with similar [3 + 6] POC analogues.[3b,5a,20]

HPOC-1 in tetrahydrofuran (THF) displayed absorption bands at 295 and 357 nm, similar to those of DBD, Fig. S21.† The molar absorption coefficient of $3.9 \times 10^4$ L mol$^{-1}$ cm$^{-1}$ at 357 nm for the cage is bigger than that of DBD ($2.0 \times 10^4$ L mol$^{-1}$ cm$^{-1}$). Upon excitation at 357 nm for DBD, a broad emission band with the maximum at 408 and 430 nm appears, Fig. S22,† corresponding to a low fluorescence quantum yield of 1.6% (calculated with quinine sulfate as the standard). In contrast, a strong emission band at 403 nm was observed for HPOC-1 under the same excitation conditions with the fluorescence quantum yield as high as 63.4% due to the formation of an imine bond,[13c,k] exceeding that of most organic cage compounds.[3a,14b] Additionally, transient fluorescence spectra showed that HPOC-1 has a higher fluorescence lifetime (1.67 ns) than DBD (1.09 ns), Fig. S23.† Since few POCs were revealed to show circularly polarized luminescence (CPL), a typical characteristic of the excited states of chiral systems with application potential in 3D display technology, optoelectronic devices and chiral sensing,[14d,f] the present fluorescence heterochiral HPOC-1 enantiomers composed of the binaphthol moiety therefore inspire us to investigate their CPL properties. As shown in Fig. 2c, (*S*,*R*)-HPOC-1 in THF exhibited a broad positive emission in the range of 380–500 nm with the maximum at 425 nm. However, the CPL profile of (*R*,*S*)-HPOC-1 shows a mirror-image with that of (*S*,*R*)-HPOC-1. The CPL dissymmetry factor ($g_{lum}$) was calculated to be $\pm 3.3 \times 10^{-4}$. This value is similar to that of analogous POCs such as 6M-2 and T-FRP 1.[14a,b]

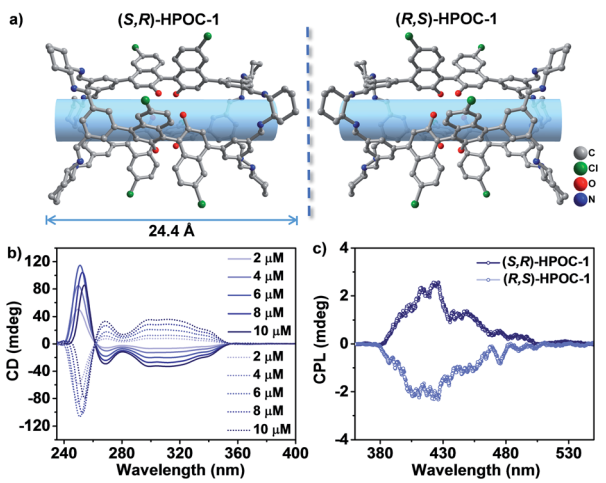


Fig. 2 (a) Single crystal structures of HPOC-1. Hydrogen atoms and ethoxy groups are omitted for clarity. (b) The CD spectra of (*S*,*R*)-HPOC-1 (solid line) and (*R*,*S*)-HPOC-1 (dotted line) with the concentrations of 2.0–10.0 μM in THF. (c) The CPL spectra of HPOC-1 (100.0 μM) in THF.

Incorporation of two kinds of chiral building blocks into HPOC-1 provides a new heterochiral host for enantioselective recognition of chiral molecules in solution. Herein, CD spectroscopy was employed to monitor the potential interaction between heterochiral HPOC-1 and chiral small molecules since this technique is able to directly discriminate molecules with different absolute configurations and ee quantitation according to visual signals, superior to fluorescence and NMR techniques.[13a,b,13j] In the present case, a series of chiral small molecules, including carvone, 1-phenylethanol, limonene, tartaric acid and pinene, were screened to probe the chiral recognition potential of HPOC-1. Gradual introduction of D-carvone resulted in the continuous decrease of the CD signal of (*S*,*R*)-HPOC-1 at 250 nm, Fig. 3a. In good contrast, a tiny CD change was found upon the introduction of L-carvone, Fig. 3b and c. These results imply the existence of specific interaction between (*S*,*R*)-HPOC-1 and D-carvone rather than L-carvone. In addition, upon increasing the D-carvone concentration from 0 to 240.0 μM, the CD signal at 250 nm for (*S*,*R*)-HPOC-1 solution decreased in a much faster manner than that of the control without POC molecules, supporting the presence of enantioselective recognition of this cage toward D-carvone, Fig. S24.† Such a phenomenon was also observed in the chiral recognition test using (*R*,*S*)-HPOC-1 towards L-carvone, Fig. 3d–3f. For the other four chiral substrates including 1-phenylethanol, tartaric acid, limonene and pinene, Fig. S25 and Table S4,† almost no obvious CD change was observed for (*S*,*R*)-HPOC-1, indicating the specificity of the chiral recognition of this POC towards D-carvone. These results imply the existence of specific interaction between (*S*,*R*)-HPOC-1 and D-carvone rather than L-carvone. In addition, a titration experiment of carvone with (*S*,*S*)-DBD at three-times the concentration of (*S*,*R*)-HPOC-1 was carried out. As shown in Fig. S26,† the CD signal changes for the solution of monomer (*S*,*S*)-DBD upon adding D- and L-carvone are similar to those of the cage, indicating that this monomer can also enantioselectively recognize D-carvone rather than L-carvone. Similar enantioselective recognition phenomena of the cage and monomer towards carvone are due possibly to the presence of 1,1′-binaphthalene moieties. However, at the same concentration of 1,1′-binaphthalene moieties for the solution of (*S*,*R*)-HPOC-1 and (*S*,*S*)-DBD, the slope absolute value of the fitting line between the CD signal intensity and the concentration of chiral D-carvone for the cage (−0.124) is much bigger than that of the monomer (−0.075), indicating the better enantioselectivity of the former species. This most probably originates from the superiority of the cage-like molecular structure which provides stronger interaction with the chiral substrate. Similar to (*S*,*R*)-HPOC-1, no obvious CD change is observed for (*S*,*S*)-DBD upon adding 1-phenylethanol enantiomers (as a representative of the used chiral substrates except carvone), Fig. S27.†

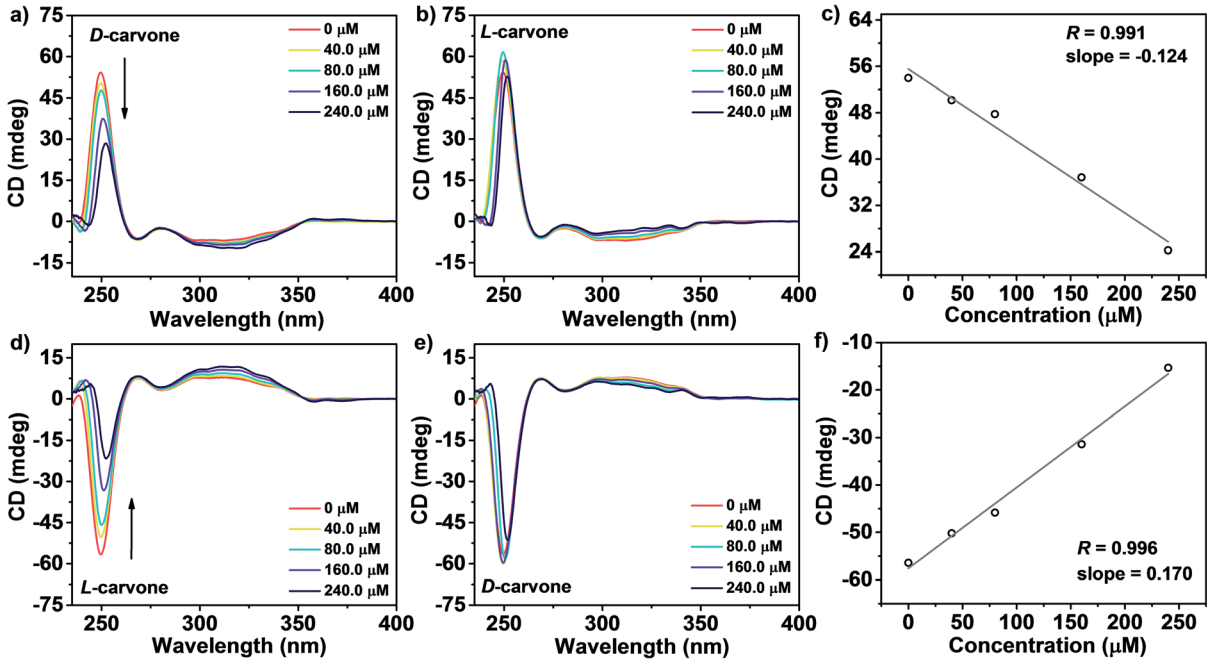


Fig. 3 CD spectra of (*S*,*R*)-HPOC-1 (2.0 μM) with different concentrations of D-carvone (a) and L-carvone (b). (c) The CD intensity at $\lambda = 250$ nm *vs.* the D-carvone concentration (0–240.0 μM). The CD spectra of (*R*,*S*)-HPOC-1 (2.0 μM) with different concentrations of (d) L-carvone and D-carvone (e). (f) The CD intensity at $\lambda = 250$ nm *vs.* the L-carvone concentration (0–240.0 μM).

These results indicate that cage (*S*,*R*)-HPOC-1 has better chiral recognition properties than monomer (*S*,*S*)-DBD.

To elucidate the monitored enantioselective recognition mechanism, molecular simulations were conducted on the (*S*,*R*)-HPOC-1 host and two enantiomeric analytes using DFT calculations. The optimized molecular structure of (*S*,*R*)-HPOC-1 bound with D-carvone shows that protons on the D-carvone point toward the face of the binaphthol moiety with atom-to-plane distances of 2.620 and 3.046 Å (Fig. S28†), respectively, indicating the presence of CH···π interactions between the cage and guest. This point was further supported by the observation of a proton signal shift in the $^1$H NMR spectrum of a mixture of (*S*,*R*)-HPOC-1 and D-carvone in comparison with that of the control, Fig. S29.† The CH–π interaction may affect the $\pi \rightarrow \pi^*$ transitions of the binaphthol moieties, leading to the change of the intensity of the CD peak at 250 nm. Furthermore, the binding energy of (*S*,*R*)-HPOC-1 and the D-carvone molecule is −102.5 kcal mol$^{-1}$, indicating the presence of binding interaction. Instead, a unstable state between (*S*,*R*)-HPOC-1 and the L-carvone molecule is suggested by the high value of binding energy (807.3 kcal mol$^{-1}$). In contrast to the obvious CD response of (*S*,*R*)-HPOC-1 towards D-carvone, we hypothesize that the non-enantioselective recognition effect of POC for L-carvone might be attributed to the much weaker interaction strength between the host and chiral guest, as indicated by the absence of an optimized structure for (*S*,*R*)-HPOC-1 in the presence of L-carvone in a 1 : 1 ratio. However, the exact reason is still not clear at this stage.

At the end of this section, it is worth noting that a series of CD spectra of (*S*,*R*)-HPOC-1 with the addition of a mixture of rac-carvone with different ee values were collected, Fig. S30a.† A good linear relationship between CD signal intensity at 250 nm and ee value was observed, Fig. S30b.† According to this standard working curve, it is easy to determine the enantiomeric excess of carvone. This point is further supported by the fact that the experimental results for three rac-carvone samples are consistent with the theoretical values, Table S5.†

## Conclusions

In summary, enantioselective assembly of new heterochiral functional materials from two kinds of enantiomeric building blocks has been clearly established. The enantioselective recognition mechanism involved in the self-assembly of building blocks has guaranteed the clean formation of a pair of heterochiral porous organic cage enantiomers with circularly polarized luminescence property. This new POC possesses enantioselective recognition capability towards chiral substrates according to the circular dichroism data. This work no doubt provides a new perspective towards constructing heterochiral POCs and therefore should benefit the chemistry of chiral self-assemblies.

## Data availability

The datasets supporting this article have been uploaded as part of the ESI.†

## Author contributions

C. Liu performed the experiments; J. Jiang, H. Wang and C. Liu conceived and supervised the project; Y. Jin, D. Qi and X. Ding

performed theoretical calculations; J. Jiang, H. Wang, C. Liu and H. Ren linked experiments and analysis; and all the authors discussed and wrote the manuscript.

## Conflicts of interest

There are no conflicts to declare.

## Acknowledgements

Financial support from the National Natural Science Foundation (NSF) of China (No. 22175020, 21631003 and 21805005), the Fundamental Research Funds for the Central Universities (No. FRF-BD-20-14A), and the University of Science and Technology Beijing, is gratefully acknowledged.

## References

1 (*a*) M. Liu, L. Zhang, A. Little Marc, V. Kapil, M. Ceriotti, S. Yang, L. Ding, L. Holden Daniel, R. Balderas-Xicohténcatl, D. He, R. Clowes, Y. Chong Samantha, G. Schütz, L. Chen, M. Hirscher and I. Cooper Andrew, *Science*, 2019, **366**, 613–620; (*b*) G. Zhang, B. Hua, A. Dey, M. Ghosh, B. A. Moosa and N. M. Khashab, *Acc. Chem. Res.*, 2021, **54**, 155–168; (*c*) K. Acharyya and P. S. Mukherjee, *Angew. Chem., Int. Ed.*, 2019, **58**, 8640–8653; (*d*) K. Jie, Y. Zhou, E. Li and F. Huang, *Acc. Chem. Res.*, 2018, **51**, 2064–2072; (*e*) R. D. Mukhopadhyay, Y. Kim, J. Koo and K. Kim, *Acc. Chem. Res.*, 2018, **51**, 2730–3273; (*f*) X. Zhao, Y. Liu, Z.-Y. Zhang, Y. Wang, X. Jia and C. Li, *Angew. Chem., Int. Ed.*, 2021, **60**, 17904–17909; (*g*) H.-H. Huang, K. S. Song, A. Prescimone, A. Aster, G. Cohen, R. Mannancherry, E. Vauthey, A. Coskun and T. Šolomek, *Chem. Sci.*, 2021, **12**, 5275–5285.

2 (*a*) M. Mastalerz, *Acc. Chem. Res.*, 2018, **51**, 2411–2422; (*b*) F. Beuerle and B. Gole, *Angew. Chem., Int. Ed.*, 2018, **57**, 4850–4878; (*c*) G. Zhang and M. Mastalerz, *Chem. Soc. Rev.*, 2014, **43**, 1934–1947.

3 (*a*) H. Wang, Y. Jin, N. Sun, W. Zhang and J. Jiang, *Chem. Soc. Rev.*, 2021, **50**, 8874–8886; (*b*) C. Liu, K. Liu, C. Wang, H. Liu, H. Wang, H. Su, X. Li, B. Chen and J. Jiang, *Nat. Commun.*, 2020, **11**, 1047; (*c*) X. Yang, J.-K. Sun, M. Kitta, H. Pang and Q. Xu, *Nat. Catal.*, 2018, **1**, 214–220.

4 (*a*) K. Kataoka, T. D. James and Y. Kubo, *J. Am. Chem. Soc.*, 2007, **129**, 15126–15127; (*b*) G. Zhang, O. Presly, F. White, I. M. Oppel and M. Mastalerz, *Angew. Chem., Int. Ed.*, 2014, **53**, 5126–5130; (*c*) S. Klotzbach and F. Beuerle, *Angew. Chem., Int. Ed.*, 2015, **54**, 10356–10360; (*d*) K. Ono, K. Johmoto, N. Yasuda, H. Uekusa, S. Fujii, M. Kiguchi and N. Iwasawa, *J. Am. Chem. Soc.*, 2015, **137**, 7015–7018; (*e*) S. Ivanova, E. Köster, J. J. Holstein, N. Keller, G. H. Clever, T. Bein and F. Beuerle, *Angew. Chem., Int. Ed.*, 2021, **60**, 17455–17463.

5 (*a*) C. Liu, W. Li, Y. Liu, H. Wang, B. Yu, Z. Bao and J. Jiang, *Chem. Eng. J.*, 2022, **428**, 131129; (*b*) Y. Lei, Q. Chen, P. Liu, L. Wang, H. Wang, B. Li, X. Lu, Z. Chen, Y. Pan, F. Huang and H. Li, *Angew. Chem., Int. Ed.*, 2021, **60**, 4705–4711; (*c*) Y. Chen, G. Wu, B. Chen, H. Qu, T. Jiao, Y. Li, C. Ge, C. Zhang, L. Liang, X. Zeng, X. Cao, Q. Wang and H. Li, *Angew. Chem., Int. Ed.*, 2021, **60**, 18815–18820; (*d*) Z. Sun, P. Li, S. Xu, Z.-Y. Li, Y. Nomura, Z. Li, X. Liu and S. Zhang, *J. Am. Chem. Soc.*, 2020, **142**, 10833–10840; (*e*) X. Tang, Z. Li, H. Liu, H. Qu, W. Gao, X. Dong, S. Zhang, X. Wang, A. C. H. Sue, L. Yang, K. Tan, Z. Tian and X. Cao, *Chem. Sci.*, 2021, **12**, 11730–11734.

6 (*a*) C. Zhang, Q. Wang, H. Long and W. Zhang, *J. Am. Chem. Soc.*, 2011, **133**, 20995–21001; (*b*) Q. Wang, C. Yu, C. Zhang, H. Long, S. Azarnoush, Y. Jin and W. Zhang, *Chem. Sci.*, 2016, **7**, 3370–3376; (*c*) S. Lee, A. Yang, T. P. Moneypenny and J. S. Moore, *J. Am. Chem. Soc.*, 2016, **138**, 2182–2185.

7 (*a*) T. Mitra, K. E. Jelfs, M. Schmidtmann, A. Ahmed, S. Y. Chong, D. J. Adams and A. I. Cooper, *Nat. Chem.*, 2013, **5**, 276–281; (*b*) Z. Wang, N. Sikdar, S.-Q. Wang, X. Li, M. Yu, X.-H. Bu, Z. Chang, X. Zou, Y. Chen, P. Cheng, K. Yu, M. J. Zaworotko and Z. Zhang, *J. Am. Chem. Soc.*, 2019, **141**, 9408–9414; (*c*) T. Hasell and A. I. Cooper, *Nat. Rev. Mater.*, 2016, **1**, 16053; (*d*) M. Yang, F. Qiu, E.-S. M. El-Sayed, W. Wang, S. Du, K. Su and D. Yuan, *Chem. Sci.*, 2021, **12**, 13307–13315; (*e*) K. Su, W. Wang, S. Du, C. Ji, M. Zhou and D. Yuan, *J. Am. Chem. Soc.*, 2020, **142**, 18060–18072; (*f*) S. Bera, K. Dey, T. K. Pal, A. Halder, S. Tothadi, S. Karak, M. Addicoat and R. Banerjee, *Angew. Chem., Int. Ed.*, 2019, **58**, 4243–4247.

8 (*a*) A. Singh, P. Verma, D. Samanta, A. Dey, J. Dey and T. K. Maji, *J. Mater. Chem. A*, 2021, **9**, 5780–5786; (*b*) B. Mondal, K. Acharyya, P. Howlader and P. S. Mukherjee, *J. Am. Chem. Soc.*, 2016, **138**, 1709–1716; (*c*) X.-X. Gou, T. Liu, Y.-Y. Wang and Y.-F. Han, *Angew. Chem., Int. Ed.*, 2020, **59**, 16683–16689; (*d*) J.-K. Sun, W.-W. Zhan, T. Akita and Q. Xu, *J. Am. Chem. Soc.*, 2015, **137**, 7063–7066.

9 (*a*) Q. Zhu, X. Wang, R. Clowes, P. Cui, L. Chen, M. A. Little and A. I. Cooper, *J. Am. Chem. Soc.*, 2020, **142**, 16842–16848; (*b*) J.-X. Ma, J. Li, Y.-F. Chen, R. Ning, Y.-F. Ao, J.-M. Liu, J. Sun, D.-X. Wang and Q.-Q. Wang, *J. Am. Chem. Soc.*, 2019, **141**, 3843–3848; (*c*) B. Han, H. Wang, C. Wang, H. Wu, W. Zhou, B. Chen and J. Jiang, *J. Am. Chem. Soc.*, 2019, **141**, 8737–8740; (*d*) Y. Kim, J. Koo, I.-C. Hwang, R. D. Mukhopadhyay, S. Hong, J. Yoo, A. A. Dar, I. Kim, D. Moon, T. J. Shin, Y. H. Ko and K. Kim, *J. Am. Chem. Soc.*, 2018, **140**, 14547–14551.

10 H. Jędrzejewska and A. Szumna, *Chem. Rev.*, 2017, **117**, 4863–4899.

11 (*a*) Z.-Y. Gu, C.-X. Yang, N. Chang and X.-P. Yan, *Acc. Chem. Res.*, 2012, **45**, 734–745; (*b*) S.-M. Xie, Z.-J. Zhang, Z.-Y. Wang and L.-M. Yuan, *J. Am. Chem. Soc.*, 2011, **133**, 11892–11895; (*c*) A. U. Malik, F. Gan, C. Shen, N. Yu, R. Wang, J. Crassous, M. Shu and H. Qiu, *J. Am. Chem. Soc.*, 2018, **140**, 2769–2772; (*d*) Y.-J. Hou, K. Wu, Z.-W. Wei, K. Li, Y.-L. Lu, C.-Y. Zhu, J.-S. Wang, M. Pan, J.-J. Jiang, G.-Q. Li and C.-Y. Su, *J. Am. Chem. Soc.*, 2018, **140**, 18183–18191; (*e*) J.-H. Zhang, S.-M. Xie, L. Chen, B.-J. Wang, P.-G. He and L.-M. Yuan, *Anal. Chem.*, 2015, **87**, 7817–7824; (*f*) Q.-P. Zhang, Z. Wang, Z.-W. Zhang, T.-L. Zhai, J.-J. Chen, H. Ma, B. Tan and C. Zhang, *Angew. Chem., Int. Ed.*, 2021,

**60**, 12781–12785; (*g*) W. Xuan, M. Zhang, Y. Liu, Z. Chen and Y. Cui, *J. Am. Chem. Soc.*, 2012, **134**, 6904–6907.

12 (*a*) R. Ning, H. Zhou, S.-X. Nie, Y.-F. Ao, D.-X. Wang and Q.-Q. Wang, *Angew. Chem., Int. Ed.*, 2020, **59**, 10894–10898; (*b*) H. Jiang, W. Zhang, X. Kang, Z. Cao, X. Chen, Y. Liu and Y. Cui, *J. Am. Chem. Soc.*, 2020, **142**, 9642–9652; (*c*) J. Jiao, C. Tan, Z. Li, Y. Liu, X. Han and Y. Cui, *J. Am. Chem. Soc.*, 2018, **140**, 2251–2259; (*d*) T. Hong, Z. Zhang, Y. Sun, J.-J. Tao, J.-D. Tang, C. Xie, M. Wang, F. Chen, S.-S. Xie, S. Li and P. J. Stang, *J. Am. Chem. Soc.*, 2020, **142**, 10244–10249.

13 (*a*) L.-L. Wang, Z. Chen, W.-E. Liu, H. Ke, S.-H. Wang and W. Jiang, *J. Am. Chem. Soc.*, 2017, **139**, 8436–8439; (*b*) L.-L. Wang, M. Quan, T.-L. Yang, Z. Chen and W. Jiang, *Angew. Chem., Int. Ed.*, 2020, **59**, 23817–23824; (*c*) Y.-Y. Zhu, X.-D. Wu, S.-X. Gu and L. Pu, *J. Am. Chem. Soc.*, 2019, **141**, 175–181; (*d*) R.-J. Li, J. J. Holstein, W. G. Hiller, J. Andréasson and G. H. Clever, *J. Am. Chem. Soc.*, 2019, **141**, 2097–2103; (*e*) T. R. Schulte, J. J. Holstein and G. H. Clever, *Angew. Chem., Int. Ed.*, 2019, **58**, 5562–5566; (*f*) Y. Ye, T. R. Cook, S.-P. Wang, J. Wu, S. Li and P. J. Stang, *J. Am. Chem. Soc.*, 2015, **137**, 11896–11899; (*g*) C. Gropp, S. Fischer, T. Husch, N. Trapp, E. M. Carreira and F. Diederich, *J. Am. Chem. Soc.*, 2020, **142**, 4749–4755; (*h*) L. Pu, *Angew. Chem., Int. Ed.*, 2020, **59**, 21814–21828; (*i*) J. T. A. Jones, T. Hasell, X. Wu, J. Bacsa, K. E. Jelfs, M. Schmidtmann, S. Y. Chong, D. J. Adams, A. Trewin, F. Schiffman, F. Cora, B. Slater, A. Steiner, G. M. Day and A. I. Cooper, *Nature*, 2011, **474**, 367–371; (*j*) Y.-P. He, L.-B. Yuan, J.-S. Song, G.-H. Chen, Q. Lin, C. Li, L. Zhang and J. Zhang, *Chem. Mater.*, 2018, **30**, 7769–7775; (*k*) S. Yu, W. Plunkett, M. Kim and L. Pu, *J. Am. Chem. Soc.*, 2012, **134**, 20282–20285; (*l*) P. Howlader, S. Mondal, S. Ahmed and P. S. Mukherjee, *J. Am. Chem. Soc.*, 2020, **142**, 20968–20972; (*m*) G. Wu, Y. Chen, S. Fang, L. Tong, L. Shen, C. Ge, Y. Pan, X. Shi and H. Li, *Angew. Chem., Int. Ed.*, 2021, **60**, 16594–16599; (*n*) L. Cheng, P. Tian, Q. Li, A. Li and L. Cao, *CCS Chem.*, 2021, **3**, 3608–3614.

14 (*a*) H. Qu, Z. Huang, X. Dong, X. Wang, X. Tang, Z. Li, W. Gao, H. Liu, R. Huang, Z. Zhao, H. Zhang, L. Yang, Z. Tian and X. Cao, *J. Am. Chem. Soc.*, 2020, **142**, 16223–16228; (*b*) H. Qu, Y. Wang, Z. Li, X. Wang, H. Fang, Z. Tian and X. Cao, *J. Am. Chem. Soc.*, 2017, **139**, 18142–18145; (*c*) Y. Zhou, H. Li, T. Zhu, T. Gao and P. Yan, *J. Am. Chem. Soc.*, 2019, **141**, 19634–19643; (*d*) S. Zheng, J. Han, X. Jin, Q. Ye, J. Zhou, P. Duan and M. Liu, *Angew. Chem., Int. Ed.*, 2021, **60**, 22711–22716; (*e*) B. Zhao, H. Yu, K. Pan, Z. a. Tan and J. Deng, *ACS Nano*, 2020, **14**, 3208–3218; (*f*) Z. Gong, X. Zhu, Z. Zhou, S. Zhang, D. Yang, B. Zhao, Y. Zhang, J. Deng, Yi. Cheng, Y. Zheng, S. Zang, H. Kuang, P. Duan, M. Yuan, C. Chen, Y. Zhao, Y. Zhong, B. Tang and M. Liu, *Sci. China: Chem.*, 2021, **64**, 2060–2104.

15 (*a*) H. Fenniri, B.-L. Deng and A. E. Ribbe, *J. Am. Chem. Soc.*, 2002, **124**, 11064–11072; (*b*) Y. Yang, M. Xue, J.-F. Xiang and C.-F. Chen, *J. Am. Chem. Soc.*, 2009, **131**, 12657–12663.

16 (*a*) N.-T. Lin, A. Vargas Jentzsch, L. Guénée, J.-M. Neudörfl, S. Aziz, A. Berkessel, E. Orentas, N. Sakai and S. Matile, *Chem. Sci.*, 2012, **3**, 1121–1127; (*b*) M. M. Safont-Sempere, P. Osswald, M. Stolte, M. Grgne, M. Renz, M. Kaupp, K. Radacki, H. Braunschweig and F. Wgrthner, *J. Am. Chem. Soc.*, 2011, **133**, 9580–9591; (*c*) X. Liu, Z. Shi, M. Xie, J. Xu, Z. Zhou, S. Jung, G. Cui, Y. Zuo, T. Li, C. Yu, Z. Liu and S. Zhang, *Angew. Chem., Int. Ed.*, 2021, **60**, 15080–15086.

17 (*a*) D. E. Fagnani, M. J. Meese Jr, K. A. Abboud and R. K. Castellano, *Angew. Chem., Int. Ed.*, 2016, **55**, 10726–10731; (*b*) K. Aratsu, R. Takeya, B. R. Pauw, M. J. Hollamby, Y. Kitamoto, N. Shimizu, H. Takagi, R. Haruki, S.-i. Adachi and S. Yagai, *Nat. Commun.*, 2020, **11**, 1623.

18 (*a*) T. Tateishi, T. Kojima and S. Hiraoka, *Commun. Chem.*, 2018, **1**, 20; (*b*) T. Kamada, N. Aratani, T. Ikeda, N. Shibata, Y. Higuchi, A. Wakamiya, S. Yamaguchi, K. S. Kim, Z. S. Yoon, D. Kim and A. Osuka, *J. Am. Chem. Soc.*, 2006, **128**, 7670–7678; (*c*) A. Shchyrba, M.-T. Nguyen, C. Wäckerlin, S. Martens, S. Nowakowska, T. Ivas, J. Roose, T. Nijs, S. Boz, M. Schär, M. Stöhr, C. A. Pignedoli, C. Thilgen, F. Diederich, D. Passerone and T. A. Jung, *J. Am. Chem. Soc.*, 2013, **135**, 15270–15273.

19 (*a*) D. Beaudoin, F. Rominger and M. Mastalerz, *Angew. Chem., Int. Ed.*, 2017, **56**, 1244–1248; (*b*) L. Greenaway, V. Santolini, A. Pulido, M. A. Little, B. M. Alston, M. E. Briggs, G. M. Day, A. I. Cooper and K. E. Jelfs, *Angew. Chem., Int. Ed.*, 2019, **58**, 16275–16281; (*c*) V. Abet, F. T. Szczypiński, M. A. Little, V. Santolini, C. D. Jones, R. Evans, C. Wilson, X. Wu, M. F. Thorne, M. J. Bennison, P. Cui, A. I. Cooper, K. E. Jelfs and A. G. Slater, *Angew. Chem., Int. Ed.*, 2020, **59**, 16755–16763; (*d*) P. Wagner, F. Rominger, W.-S. Zhang, J. H. Gross, S. M. Elbert, R. R. Schröder and M. Mastalerz, *Angew. Chem., Int. Ed.*, 2021, **60**, 8896–8904; (*e*) L.-L. Yan, C.-H. Tan, G.-L. Zhang, L.-P. Zhou, J.-C. Bünzli and Q.-F. Sun, *J. Am. Chem. Soc.*, 2015, **137**, 8550–8555; (*f*) P. Li, Z. Sun, J. Chen, Y. Zuo, C. Yu, X. Liu, Z. Yang, L. Chen, E. Fu, W. Wang, J. Zhang, Z. Liu, J. Hu and S. Zhang, *J. Am. Chem. Soc.*, 2022, **144**, 1342–1350; (*g*) T. Jiao, H. Qu, L. Tong, X. Cao and H. Li, *Angew. Chem., Int. Ed.*, 2021, **60**, 9852–9858.

20 A. G. Slater, M. A. Little, A. Pulido, S. Y. Chong, D. Holden, L. Chen, C. Morgan, X. Wu, G. Cheng, R. Clowes, M. E. Briggs, T. Hasell, K. E. Jelfs, G. M. Day and A. I. Cooper, *Nat. Chem.*, 2017, **9**, 17–25.

21 P. van der Sluis and A. L. Spek, *Acta Crystallogr., Sect. A: Found. Crystallogr.*, 1990, **46**, 194–201.